



RESEARCH ARTICLE

10.1029/2023JD040353

Investigating Zonal Asymmetries in Stratospheric Ozone Trends From Satellite Limb Observations and a Chemical Transport Model

Key Points:

- A longitudinal asymmetry in stratospheric ozone trends at northern high latitudes is found in satellite observations in the past two decades
- The asymmetry is particularly large in springtime and the TOMCAT chemistry transport model well reproduces the pattern
- Changes in polar wave activity and in the position and strength of the polar vortex are found to be relevant to explain this pattern

Supporting Information:

Supporting Information may be found in the online version of this article.

Correspondence to:

C. Arosio,
carloarosio@iup.physik.uni-bremen.de

Citation:

Arosio, C., Chipperfield, M. P., Rozanov, A., Weber, M., Dhomse, S., Feng, W., et al. (2024). Investigating zonal asymmetries in stratospheric ozone trends from satellite limb observations and a chemical transport model. *Journal of Geophysical Research: Atmospheres*, 129, e2023JD040353. <https://doi.org/10.1029/2023JD040353>

Received 3 NOV 2023

Accepted 30 MAR 2024

Author Contributions:

Conceptualization: M. P. Chipperfield,

A. Rozanov, M. Weber, J. P. Burrows

Data curation: C. Arosio, S. Dhomse, W. Feng, G. Jaross

Formal analysis: X. Zhou

Funding acquisition: C. Arosio,

A. Rozanov, J. P. Burrows

Investigation: C. Arosio, M. Weber,

X. Zhou

Methodology: C. Arosio,

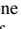





M. P. Chipperfield, A. Rozanov,

M. Weber, S. Dhomse, X. Zhou

Project administration: C. Arosio,

A. Rozanov, J. P. Burrows

Resources: M. P. Chipperfield

C. Arosio¹ , M. P. Chipperfield^{2,3} , A. Rozanov¹, M. Weber¹ , S. Dhomse^{2,3} , W. Feng² , G. Jaross⁴, X. Zhou^{2,5}, and J. P. Burrows¹ 

¹Institute of Environmental Physics, University of Bremen, Bremen, Germany, ²School of Earth and Environment, University of Leeds, Leeds, UK, ³National Centre for Earth Observation (NCEO), University of Leeds, Leeds, UK, ⁴NASA Goddard Space Flight Center, Greenbelt, MD, USA, ⁵School of Atmospheric Sciences, Chengdu University of Information Technology, Chengdu, China

Abstract This study investigates the origin of a zonal asymmetry in stratospheric ozone trends at northern high latitudes, identified in satellite limb observations over the past two decades. We use a merged data set consisting of ozone profiles retrieved at the University of Bremen from SCIAMACHY and OMPS-LP measurements to derive ozone trends. We also use TOMCAT chemical transport model (CTM) simulations, forced by ERA5 reanalyses, to investigate the factors that drive the asymmetry observed in the long-term changes. By studying seasonally and longitudinally resolved observation-based ozone trends, we find, especially during spring, a well-pronounced asymmetry at polar latitudes with values up to +6 % per decade over Greenland and −5 % per decade over western Russia. The control CTM simulation agrees well with these observed trends, whereas sensitivity simulations indicate that chemical mechanisms involved in the production and removal of ozone, or their changes, are unlikely to explain the observed behavior. The decomposition of TOMCAT ozone time series and ERA5 geopotential height into the first two wavenumber components shows a clear correlation between the two variables in the middle stratosphere and demonstrates a weakening and a shift in the wavenumber-1 planetary wave activity over the past two decades. Finally, the analysis of the polar vortex position and strength points to a decadal oscillation with a reversal pattern at the beginning of the century. The same is found in the ozone trend asymmetry. This further stresses the link between changes in the polar vortex position and the identified ozone trend pattern.

Plain Language Summary Monitoring long-term ozone changes in the stratosphere is important and aims to assess the ozone layer's evolution in response to the Montreal Protocol and climate change. In this study, we investigate the origin of a zonal asymmetry in stratospheric ozone trends over the past two decades, which was identified at northern polar latitudes by analyzing satellite observations. To this aim, we use a merged data set consisting of ozone profiles retrieved at the University of Bremen from SCIAMACHY and OMPS-LP measurements to derive ozone trends. We also use TOMCAT chemical transport model (CTM) simulations to investigate the factors that determine the asymmetry observed in long-term ozone changes. The asymmetry is largest in springtime, and the CTM simulation agrees well with the observation-based trends. Sensitivity simulations indicate that chemical mechanisms involved in the production and destruction of ozone are unlikely to explain the observed pattern. In contrast, changes in atmospheric dynamics are found to be relevant. Our analysis of the polar vortex position and strength shows a cyclical pattern that reverses its phase near the year 2000. We observe this same pattern in the ozone trend asymmetry.

1. Introduction

The variations of the ozone concentration as a function of time, altitude and latitude are explained by several dynamical, chemical and photochemical processes (e.g., Seinfeld & Pandis, 2016; WMO, 2022). In the lower stratosphere, where the chemical lifetime is measured in years, except during polar spring, ozone is transported from the tropics to high latitudes, and it is affected by changes in atmospheric dynamics. In the upper stratosphere ozone has a relatively short photochemical lifetime, implying that changes in the transport of long-lived chemical species and in temperature play an important role in determining ozone concentrations at those levels.

© 2024. The Authors.

This is an open access article under the terms of the [Creative Commons Attribution License](https://creativecommons.org/licenses/by/4.0/), which permits use,

distribution and reproduction in any medium, provided the original work is properly cited.

Software: C. Arosio, M. P. Chipperfield, S. Dhomse, W. Feng

Supervision: M. P. Chipperfield, A. Rozanov, M. Weber, G. Jaross, J. P. Burrows

Writing – original draft: C. Arosio

Writing – review & editing: C. Arosio, M. P. Chipperfield, A. Rozanov, M. Weber, S. Dhomse, W. Feng, G. Jaross, X. Zhou, J. P. Burrows

Stratospheric circulation comprises an upper branch of the Brewer–Dobson circulation (BDC) involving upwelling in the tropics, meridional poleward transport, and then descent in the polar regions. The lower branch of the BDC has a more rapid meridional poleward transport on isentropic surfaces (Butchart, 2014). This circulation is driven by wave breaking in the stratosphere, mostly of planetary-scale Rossby waves, and is therefore subject to strong inter-annual variability. The wave breaking happens in the so called “surf zone” at the edge of the polar vortex so that its position and vertical structure has an indirect impact on the BDC, which in turn affects the vortex position and strength (McIntyre & Palmer, 1984). An acceleration of the stratospheric mean mass transport has been predicted by several model studies (e.g., Garcia & Randel, 2008), but strong inter-annual variations prevent a robust detection of this trend from observations. In addition there may be decadal oscillations. A large inter-annual variability also characterizes the polar vortex, with climate models not agreeing on whether it will weaken or strengthen during the 21st century (Karpechko et al., 2022). Several studies have addressed decadal changes of the polar vortex position and strength (e.g., Seviour, 2017; Zhang et al., 2016), pointing out a vortex weakening and shift of its mean position toward Eurasia, particularly at the end of the last century. In contrast, Hu et al. (2018) presented a strengthening of the stratospheric polar vortex over the last two decades that could be related to a weakening of the propagation of wavenumber-one wave fluxes. This was connected by the authors to sea-surface temperature warming over the north Pacific sector.

Among various anthropogenic influences on stratospheric ozone, the two most relevant are the release of halogen-containing ozone-depleting substances (ODSs) and of greenhouse gases (GHGs). Industrial production of ODSs, especially chlorofluorocarbons (CFCs), has been regulated since the adoption of the Montreal Protocol and its amendments. Reduced emissions during the 1990s are expected to lead to a recovery of the ozone layer globally (e.g., WMO, 2018; WMO, 2022). On the other hand, the increasing concentration of GHGs such as CO_2 and CH_4 in the troposphere is causing a cooling of the stratosphere through radiative transfer feedback. This cooling affects ozone chemistry in the upper stratosphere because the catalytic cycles removing ozone have rate coefficients that are dependent on temperature (e.g., Waugh et al., 2009). At the same time, the termolecular reaction $O_2 + O + M \rightarrow O_3 + M$ has a rate inversely proportional to temperature so that the cooling also accelerates ozone production (Groves et al., 1978).

The coupling between these chemical and dynamical processes controlling stratospheric ozone is expected to have a complex spatial structure, varying in altitude, latitude, longitude and time. Therefore, to study long-term variations of the ozone field there is a need for consistent long-term time series with a good temporal and spatial coverage over the whole globe.

Single instrument time series are generally inadequate to study long-term changes in ozone vertical profiles and test our understanding of the impact of natural phenomena and anthropogenic activities on atmospheric ozone. Several studies have used merged satellite data sets to investigate stratospheric ozone trends, but the majority of them have focused only on zonal mean changes (e.g., WMO, 2022). By exploiting the dense spatial sampling provided by limb observations, Arosio et al. (2019) and Sofieva et al. (2021) looked at longitudinally resolved trends and highlighted the presence of zonal asymmetries, especially at northern high latitudes. In particular, they identified a bi-polar structure poleward of $60^\circ N$, having positive values over the Atlantic/Greenland sector and close to zero or negative changes over Siberia.

As discussed in the following paragraphs, some studies using model simulations and satellite data sets have also shown zonal asymmetries in the BDC and its impact on the distribution of trace gases and ozone trends in winter-time at northern high latitudes. Most studies focused on total ozone column measurements.

Longitudinally varying changes in total ozone were already pointed out in the study by Hood and Zaff (1995), who investigated total ozone at northern mid-latitudes during winter in the 1980s using TOMS measurements. The authors identified the typical asymmetric ozone distribution related to quasi-stationary planetary waves, that is, a pronounced maximum over eastern Russia related to the Aleutian low and a secondary maximum over eastern Canada associated with the Icelandic low. In addition, a distinct longitudinal dependence of the mid-latitude ozone trends over this period was identified: the largest negative trends (-40 DU over the considered decade) occurred over Russia and western Pacific, whereas positive trends were found over the northern Atlantic sector. Another study using TOMS data was performed by Peters and Entzian (1999), who investigated decadal total ozone changes in the months December–February over the period 1979–1992 in the northern hemisphere. They found a strong anti-correlation between the long-term total ozone changes and the 300-hPa geopotential height (GPH) changes. This means that decadal changes in the UTLS dynamics led to longitude-dependent

changes in the total ozone. More recently, Coldewey-Egbers et al. (2022) showed pronounced asymmetries in total ozone trends by using a merged total column data record over the period 1995–2020, with a maximum over the Atlantic sector at 60°N.

Asymmetries in the ozone climatology were investigated by Bari et al. (2013) using models, reanalysis, and satellite data and focusing on the northern mid-latitudes in winter. The authors stressed the importance of a 3-D approach in studying the BDC. They found that the distribution of winds and trace gases is related to the zonal wavenumber-1 pattern in geopotential height (GPH) observed in the northern hemispheric stratosphere during winter at high and mid-latitudes. They showed that air masses are driven southwards and upwards to the upper stratosphere over the Pacific ocean, whereas over Europe and Asia the flow is northward and downward.

More recently, Kozubek et al. (2015) investigated the meridional component of stratospheric winds as a function of altitude at northern mid-latitudes to study its longitudinal dependency. A well-defined two-core structure with opposite wind directions was identified at 10 hPa in the northern hemisphere, related to the Aleutian pressure high at 10 hPa. They also computed meridional wind changes over two periods: 1970–1995 and 1996–2012. They found that meridional wind trends are negative in the first period and positive in the second period, that is, the two-core structure became stronger in the later two decades. As a follow up, Kozubek et al. (2017) investigated the long-term variations of stratospheric winds over the whole globe at 10 hPa using four reanalysis data sets. The trends were reported for winter months before and after the ozone trend turnaround point at the end of the 1990s. They found hints of an acceleration of the BDC and change in the ozone trend asymmetries before and after 1997.

Within this framework and in light of the findings in Arosio et al. (2019) and Sofieva et al. (2021), the present paper aims to analyze vertically and longitudinally resolved ozone trends from satellite observations and to exploit simulations from the TOMCAT chemistry transport model (CTM) to identify the mechanisms driving the observed zonal asymmetry in the ozone trends in the period 2004 to 2021. Sect. 2 introduces the satellite data set used in this study and the TOMCAT CTM. Sect. 3 shows a comparison of the measured and simulated ozone anomalies and of the respective zonally and longitudinally resolved trends, where the asymmetry is evident at northern high latitudes. Sect. 4 presents the results of TOMCAT runs, which were designed to assess the impact of chemical processes on the observed longitudinally asymmetric pattern in ozone trends. In Sect. 5 we explore in more detail the seasonally resolved long-term changes in ozone and temperature, which leads to Sect. 6 where geopotential height and ozone fields are decomposed into wavenumber-1 and -2 to assess similarities in their behavior. Finally, in Sect. 7 we present some potential vorticity trends to further investigate changes in the polar vortex over the past two decades, followed by concluding remarks in Sect. 8.

2. Data Sets

2.1. Satellite Observations

The merged satellite data set consisting of observations from the SCanning Imaging Absorption spectromETER for Atmospheric CHartographY (SCIAMACHY) and the Ozone Mapping and Profiler Suite - Limb Profiler (OMPS-LP) has been produced at the University of Bremen and is described in Arosio et al. (2019). Here, it will be referred to as SCIA + OMPS. This data set is longitudinally resolved with a grid size of 5° in latitude and 20° in longitude and has a vertical resolution of 3.3 km. The time series has been recently updated after the re-processing of the OMPS-LP data set by using improved Level 1 gridded (L1G) data. In the new L1G data version (v2.6), the NASA team implemented some calibration corrections, a wavelength registration adjustment, and an improved pointing correction. The primary aim of the re-processing was the removal of the positive drift identified in the previous OMPS-LP ozone product with respect to independent time series (Kramarova et al., 2018), for example, from the Microwave Limb Sounder (MLS). The latter has proven its long-term stability in previous studies, for example, Hubert et al. (2016). We define the drift as the linear trend of the relative difference between OMPS-LP and MLS.

The drift with respect to MLS time series is shown in Figure 1. The left panel refers to the OMPS-LP time series retrieved using L1G v2.5 data, whereas the right panel refers to the updated time series, based on L1G v2.6 data. The comparison between the left and the right panel shows that the strong positive drift with respect to MLS has been significantly reduced, particularly above 35 km. The striped areas indicate values which are lower than the respective 2σ uncertainty, that is, they are not statistically significant at 95% confidence level. Drift values are still significant at some altitude-latitudes but generally with values half as large as in the previous data version. This

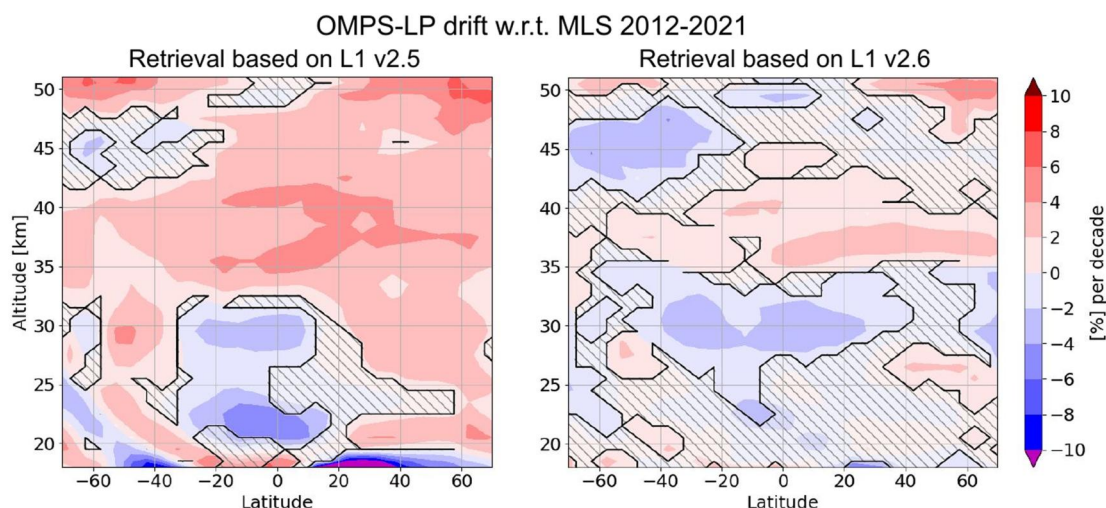


Figure 1. Drift of the OMPS-LP ozone product retrieved at the University of Bremen with respect to MLS during the period 2012–2021 in % per decade. Left panel: using L1G v2.5 data. Right panel: using L1G v2.6 data. Striped areas are non-significant at 2σ .

result provides improved confidence in the scientific value of the ozone trends derived from the SCIA + OMPS merged time series.

2.2. TOMCAT Chemical Transport Model

TOMCAT/SLIMCAT is a three-dimensional off-line chemical transport model (CTM) (Chipperfield, 2006). The model is forced by winds and temperatures from meteorological analyses, which in this study are taken from the European Center for Medium-Range Weather Forecasts (ECMWF) reanalysis v5 (ERA5). Once the atmospheric transport and temperatures are prescribed, the model calculates the abundances of chemical species in the troposphere and stratosphere. A full-chemistry reference run was used as baseline for this study and other dedicated runs were produced. The resolution of the model was $2.8^\circ \times 2.8^\circ$ latitude and longitude, and about 1.5 km altitude in the stratosphere, and the output was interpolated to match the merged satellite data set resolution. Monthly averaged values are considered.

The TOMCAT CTM simulations were used in this study for three important reasons.

1. The CTM provides a continuous time series without spatial or temporal gaps so that it is possible, for example, to explore polar winter conditions, which are not sampled by limb scattering sounders;
2. The possibility to study trends going back in time until 1980s, when satellite limb observations were sparse;
3. The possibility to investigate the mechanisms that determine the trend asymmetries by running dedicated simulations using different settings.

3. Comparison With TOMCAT: Time Series and Trends

As a preliminary consistency check, we looked into the absolute bias between SCIA + OMPS and TOMCAT time series and noticed that the CTM underestimates ozone content in the upper stratosphere and overestimates it in the lower stratosphere, which is a known feature (Dhomse et al., 2021); further investigations on this issue are outside the scope of this paper. For this reason and because we are interested in ozone trends, deseasonalized (relative) anomalies of the time series were calculated and found to be in good agreement with SCIA + OMPS, as shown in Figure 2. In the lower tropical stratosphere the amplitude of the oscillations, probably due to the Quasi Biennial Oscillation (QBO), is more pronounced in TOMCAT than in SCIA + OMPS. MLS time series is also included as a reference in this plot.

We applied a multivariate linear regression model to both TOMCAT and SCIA + OMPS time series based on the Long-term Ozone Trends and Uncertainties in the Stratosphere (LOTUS) model and including several proxies. In particular, we included in the regression model traditionally employed proxies (e.g., Petropavlovskikh et al., 2019) such as the first two principal components of the QBO, the Multivariate El Niño Southern Oscillation

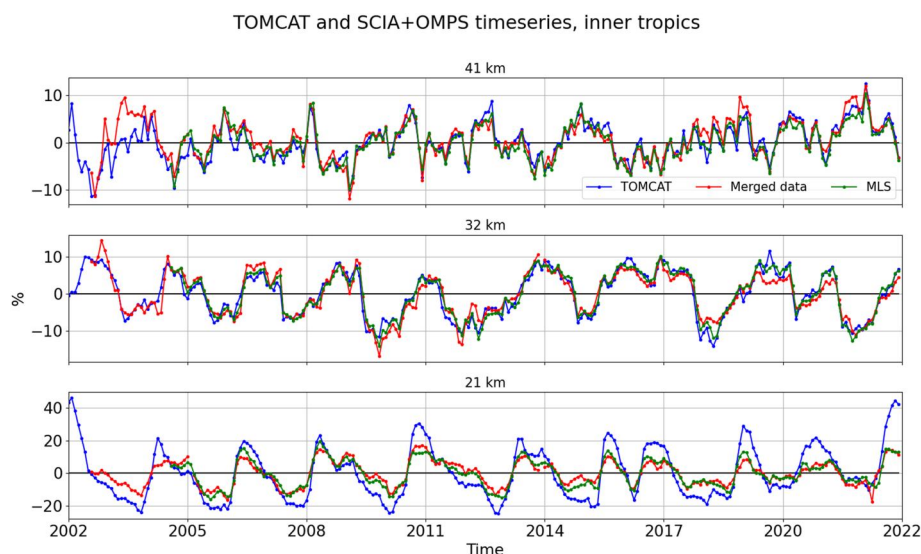


Figure 2. Deseasonalized ozone anomalies from the reference TOMCAT simulation, the merged SCIA + OMPS data set, and MLS time series in the inner tropics (5°S , 5°N) at three altitudes (41, 32 and 21 km).

(ENSO) index (MEI), and the Mg II index for solar activity. We also applied dynamical proxies such as the yearly integrated eddy heat fluxes and the Atlantic/Antarctic oscillation (AO/AAO). For a more detailed description of the proxies used we refer to Weber et al. (2022).

Due to the discrepancies found in the first year of the SCIAMACHY time series with respect to other satellite products (Sofieva et al., 2017), and because of the January 2022 Hunga Tonga volcanic eruption with its large stratospheric perturbation (Lu et al., 2023), we focus on the period 2004–2021 to study ozone trends. The resulting zonal mean ozone trends are reported in Figure 3. Striped areas in this and the following plots indicate values that are smaller than the 2σ uncertainty (non-significant).

A generally good agreement between model and observations is found with the expected positive trends in the middle and upper stratosphere related to the ongoing ozone recovery. The most significant discrepancy is located below 25 km: TOMCAT shows overall positive trends, whereas SCIA + OMPS shows negative values that are significant only in the inner tropics below 19 km. The detection of negative trends in the lower tropical and extra-tropical stratosphere has been extensively debated (Ball et al., 2018; Chipperfield et al., 2018). A possible reason for the discrepancy between TOMCAT and SCIA + OMPS in the lower stratosphere is related to ERA5 forcing, as pointed out by Li et al. (2022, 2023). In comparison to the long-term 2000–2020 ozone

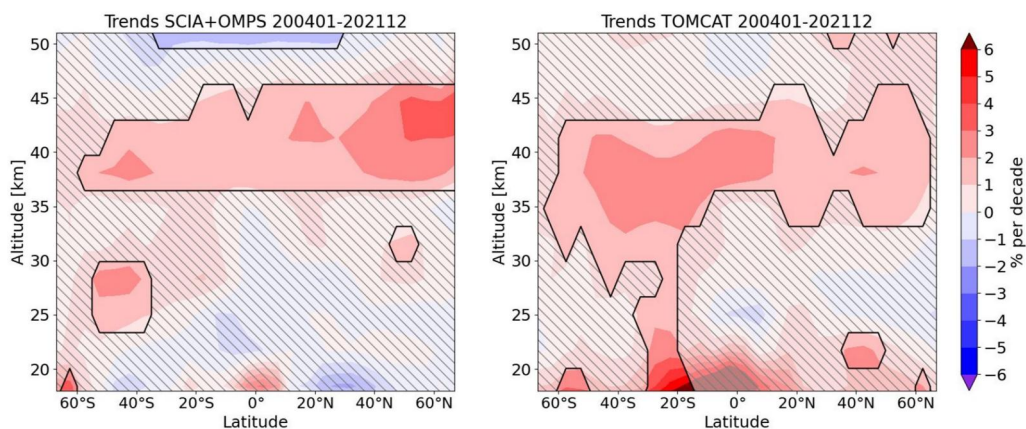


Figure 3. Zonal mean ozone trends from SCIA + OMPS on the left and from TOMCAT on the right, computed over the 2004–2021 period. Striped areas are non-significant at 2σ .

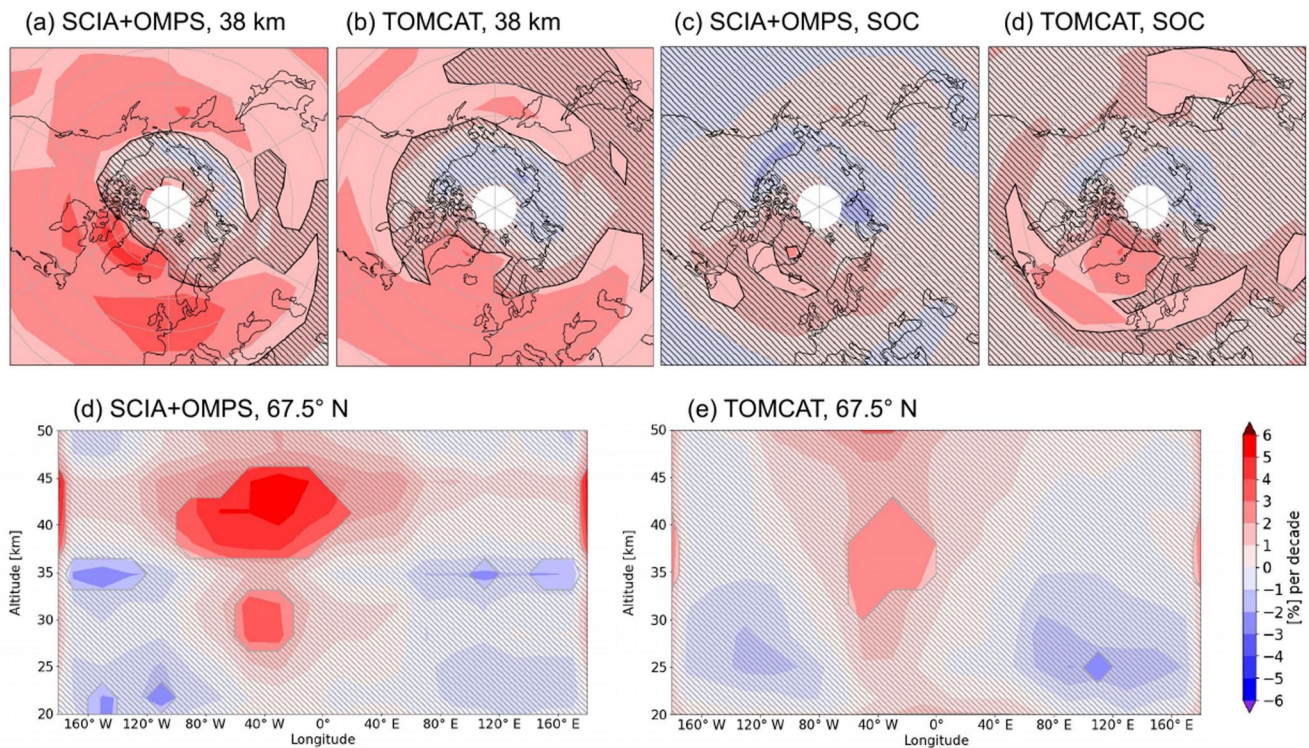


Figure 4. Top row: longitudinally resolved ozone trends (%/decade) from SCIA + OMPS and TOMCAT data sets at 38 km and for stratospheric column. Bottom row: ozone trends for a longitude-altitude cross section at 67.5°N. The striped areas denote non-significant values at 2σ level.

trends shown in Godin-Beekmann et al. (2022), trend values in the lower stratosphere are not significant and closer to zero. The negative values identified in SCIA + OMPS above 47 km are not shown by other merged data sets.

Longitudinally resolved trends in ozone from TOMCAT and SCIA + OMPS are compared in Figure 4. In the top row we note a pronounced longitudinal variability and some common patterns in CTM and in SCIA + OMPS trends, especially the longitudinal asymmetry. This asymmetry is more evident in TOMCAT, with negative (though non-significant) values over the Siberian and East-Canadian sectors, and positive values over the Atlantic sector. Considering the two sets of plots in Figure 4, we can see that the asymmetry is vertically consistent. The positive SOC trends in the Atlantic sector are significant at 2σ, especially for TOMCAT. A similar structure was also identified in the MLS time series and in the MEGRIDOP data set (Sofieva et al., 2021), as shown in Figure S1 in Supporting Information S1. Above 35 km, TOMCAT shows smaller positive values over the Atlantic sector as compared to the satellite observations. To further test the robustness of this pattern and its independence from ERA5 forcing, we compare trends from the MERRA 2 - Global Modeling Initiative (M2-GMI) CTM time series, which is forced with MERRA 2 meteorology, with TOMCAT, and found a bias in terms of absolute trend values but good agreement in terms of asymmetric pattern. These results are shown in the SI, Figure S6 in Supporting Information S1.

A TOMCAT simulation with a higher spatial resolution ($1.4^\circ \times 1.4^\circ \times 0.75$ km grid) was run to investigate whether the discrepancies between the CTM and SCIA + OMPS could be reduced. This simulation was sampled at the locations of the satellite observations to make the CTM time series more consistent with the merged data set in terms of temporal and spatial sampling. The resulting data set was re-gridded and the two parts of the time series, covering SCIAMACHY and OMPS-LP periods, respectively, were de-biased to remove the discrepancy related to the different local time of the satellite observations. The comparison of the resulting higher resolution data did not show any significant differences with respect to the standard run, neither in the trends nor in the time series (not shown here). Therefore, we use the standard run as reference in this study.

Longitudinally resolved O3 trends TOMCAT, 200401 - 202112

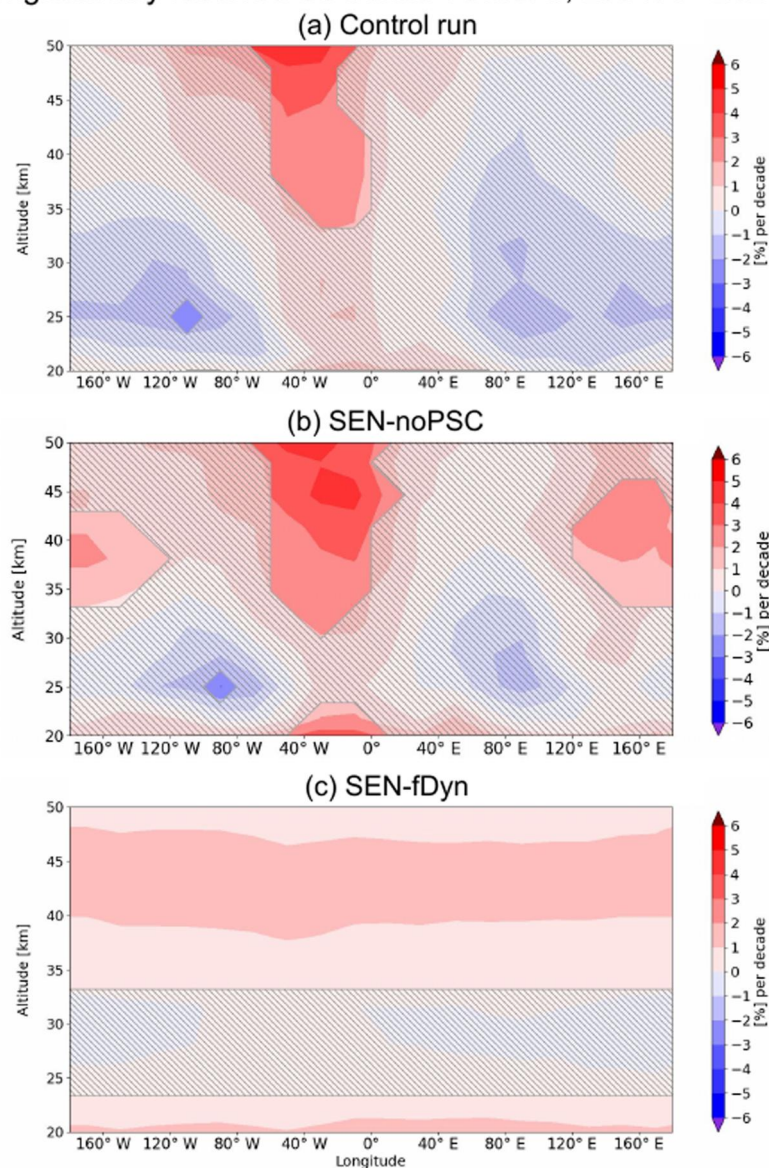


Figure 5. Longitudinally resolved ozone trend (%/decade) cross sections at 70°N over 2004–2021 for three TOMCAT scenarios: (a) reference control run, (b) PSC-inhibited scenario and (c) repeating forcing.

4. Investigation of the Potential Influence of Chemical Processes on the Trend Asymmetry

We performed two additional TOMCAT sensitivity (SEN) simulations to investigate the potential influence of chemical processes on the origin of the ozone trend asymmetry. The first simulation, SEN-fDyn, was forced using constant ERA5 data corresponding to the year from July 1999 to June 2000, which were repeated each year over the 2004–2021 period. The choice of the 1999/2000 years is arbitrary as far as a winter with an average-strong Arctic vortex is considered; we tested the use of the July 2002 to June 2003 period for the repeating forcing without finding any significant difference. In the second simulation, SEN-noPSC, polar stratospheric cloud (PSC)-related heterogeneous chemistry was inhibited by not allowing temperature to drop below 200 K in the model chemistry scheme. The results are shown in Figure 5. The longitude-altitude cross section of the ozone trends at 67.5°N over 2004–2021 from the reference full-chemistry TOMCAT (control) run is shown together with the trends for the SEN-noPSC and SEN-fDyn simulations.

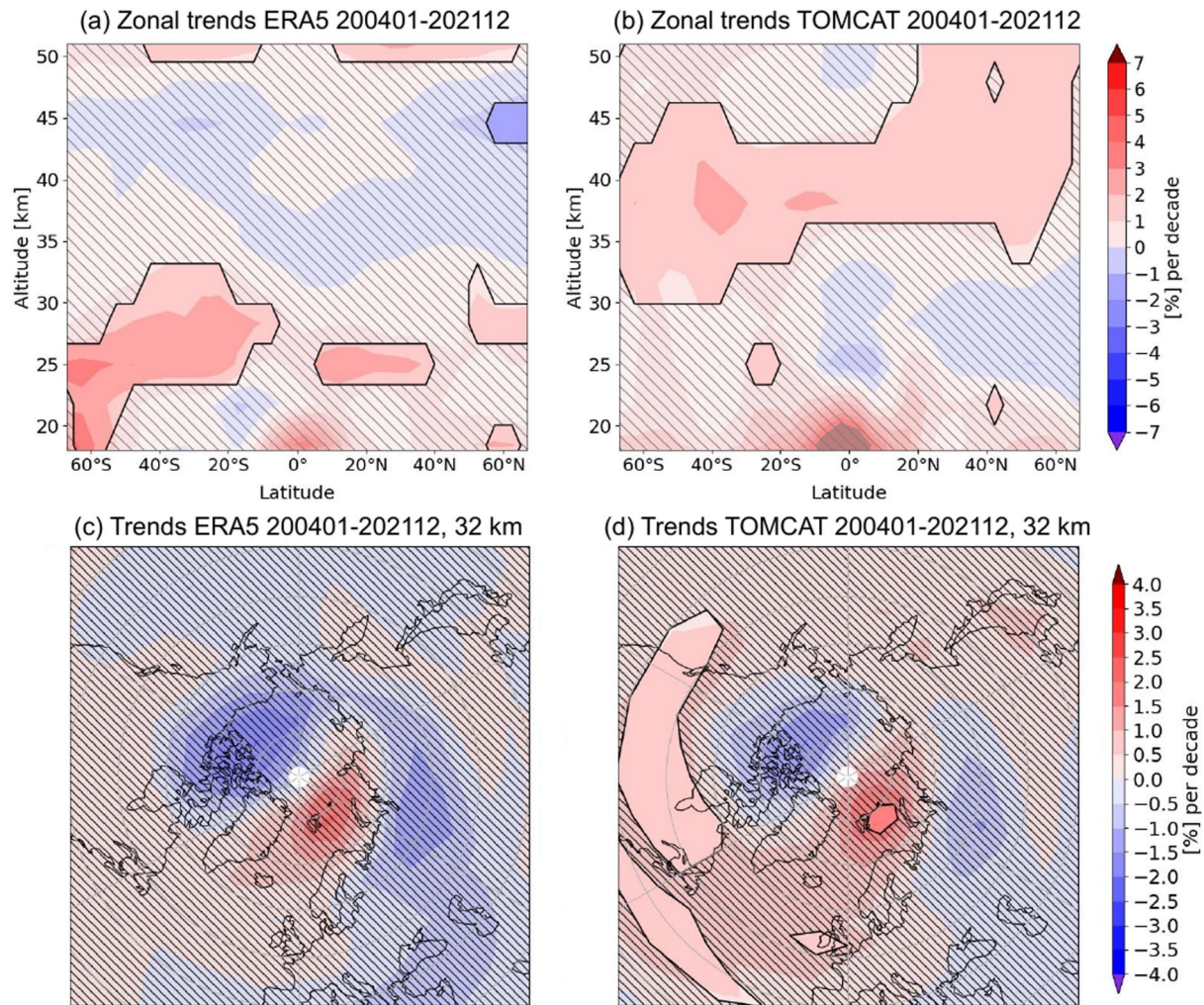


Figure 6. Panels (a) and (b) show zonal ozone trends (%/decade) for ERA5 and TOMCAT time series, respectively, over 2004–2021. Panels (c) and (d) show longitudinally resolved trends at 32 km for ERA5 and TOMCAT, respectively.

Figure 5 shows that the zonally asymmetrical trend pattern from the SEN-noPSC simulation is almost identical to the one from the control simulation. As expected, the trends over the Atlantic sector are smaller due to reduced ozone losses in the absence of PSCs. This indicates that heterogeneous chemistry does not play a significant role in producing trends that vary with longitude. To further test this hypothesis and the robustness of the zonal asymmetry we computed the ozone trends for the 2004–2019 period, that is, excluding the cold 2019/2020 Arctic winter. As shown in the SI, Figure S3 in Supporting Information S1, we did not find relevant differences, thus highlighting the robustness of the pattern.

Trend values in the 'repeating forcing' (sen-fDyn) scenario show zonal symmetry and are overall smaller with respect to the control run. In this case no long-term temperature trend is present in the forcing. This plays an important role in driving the ozone trend in the upper stratosphere. The fact that no zonal asymmetry is observed for this run indicates that gas-phase chemistry alone cannot directly explain the asymmetry in trends. However, an indirect impact of atmospheric dynamics on gas-phase chemistry cannot be excluded (Galytska et al., 2019).

We also compared the trend results computed for the TOMCAT reference run and for ERA5 ozone data. As shown in Figure 6, the zonal trends in ERA5 are significantly different from the trends shown in Figure 3, which exemplifies that ozone reanalysis data should not be used to compute long-term ozone changes unless a careful de-biasing of the time series is performed. This is discussed in for example, Simmons et al. (2014); Bernet et al. (2020); WMO (2022). Bearing in mind this caveat, we note that the longitudinally resolved trends shown in

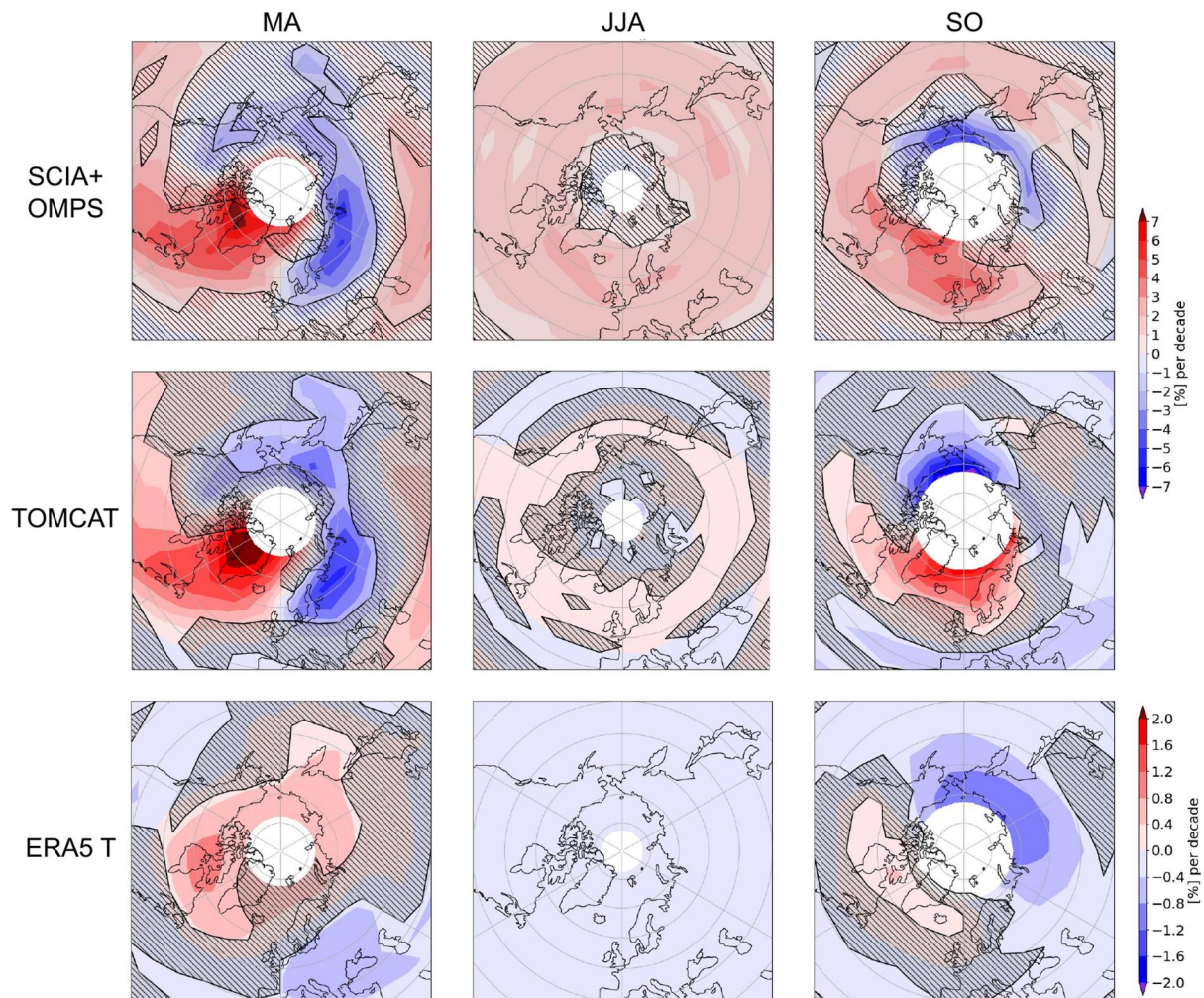


Figure 7. Seasonally resolved ozone trends (%/decade) at 32 km from SCIA + OMPS data set (top row), TOMCAT reference simulation (middle row), and ERA5 temperature (bottom row). The left column shows trends for spring (MA), the middle column for summer (JJA), and the right one for autumn (SO).

Figure 6 at 32 km have a remarkable similarity with the pattern found in TOMCAT. This provides more evidence that atmospheric dynamics is the main driver of the observed asymmetric pattern since TOMCAT is forced with ERA5 meteorology.

5. Seasonal Ozone Trends

To further investigate the longitudinal asymmetry at northern high latitudes, we analyzed seasonal trends. Two approaches to obtain seasonal time series for the SCIA + OMPS data set are described in Appendix A. In the following, we show trend values obtained by merging the two seasonally resolved single-instrument time series.

Figure 7 shows seasonal ozone trends for SCIA + OMPS (top row) and for the reference TOMCAT run (middle row) at 32 km altitude for spring (MA), summer (JJA) and autumn (SO). Only 2 months are used in spring and autumn to obtain a better coverage of the polar regions. The TOMCAT time series was masked to mirror the availability of satellite data. ERA5 temperature trends are displayed in the bottom row of Figure 7 for the same three seasons. Regarding temperature trends, we again remark here that reanalysis data are not meant to be used to compute trends. In this case, however, we are using this information for a qualitative evaluation of the agreement between the patterns. A comparison with MLS seasonal trends is reported in the SI, Figure S2 in Supporting Information S1.

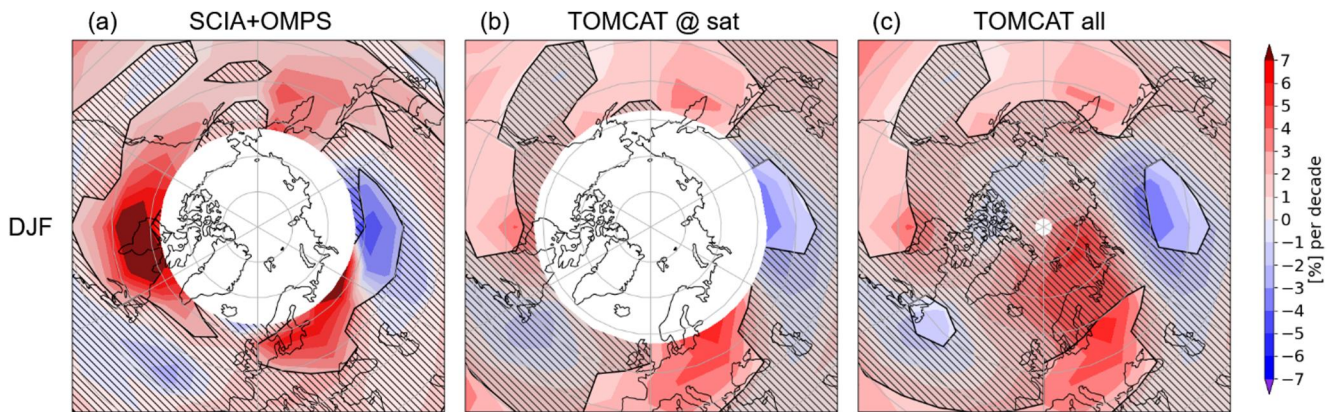


Figure 8. Seasonally resolved trends in DJF at 32 km from SCIA + OMPS (panel a) and TOMCAT. In panel (b) the TOMCAT simulation was sampled as the satellite data whereas in panel (c) the non-sampled TOMCAT time series was used to compute the trends.

During summer (JJA, middle column of Figure 7) the trend fields are fairly homogeneous over longitude, displaying significant positive values of about 1% per decade for SCIA + OMPS and close to zero for TOMCAT. In contrast, during spring (left column) and autumn (right column) the asymmetry is well pronounced. In particular, we note a strong zonal asymmetry in the spring-time trends in SCIA + OMPS that is captured very well by TOMCAT, with the positive maximum located over the North Atlantic sector. The negative values between Scandinavia and Siberia are also statistically significant (at 2σ level) for both observations and model. A similar bi-polar pattern is also found in SO, but more confined to polar latitudes and shifted in longitude. The good agreement of TOMCAT with observations also holds in this case. The time series of two points located in the maximum and minimum of the identified pattern are shown in Figure S5 in Supporting Information S1.

Regarding temperature, in summer we find a small homogeneous negative trend, whereas in spring and autumn the pattern is zonally asymmetric. However no strong correlation with the patterns observed in the ozone trends was found. In addition, we also investigated trends in ERA5 GPH for the same season, which are shown in Figure S4 in Supporting Information S1. Similar patterns as in ozone trends are visible, with the strongest asymmetry in spring and a homogeneous field during summer months.

A comparison between TOMCAT and SCIA + OMPS during winter months is more difficult as limb scattering observations do not sample polar night conditions (see Figure 8, panel (a)). SCIA + OMPS shows large positive values with maxima over Canada and Scandinavia. The CTM, sampled in the same manner as the SCIA + OMPS monthly time series, shows a comparable pattern (Figure 8, panel (b)) with less pronounced positive values. The trends calculated using the full TOMCAT profiles (non-sampled and averaged over all the model time steps) give a better picture of the two positive cores (over Canada and Scandinavia) and two negative cores (over Siberia and South of Greenland), although mostly not statistically significant.

6. Changes in GPH and Atmospheric Dynamics

One possible cause of the asymmetry in ozone trends during the last two decades is wave activity at northern high latitudes. To investigate this we analyzed the time series of GPH from ERA5. Specifically, we considered the longitudinally resolved vertical structure of the GPH field and decomposed it in wavenumber one (wave-1) and wavenumber two (wave-2) components using a fast Fourier transform (FFT). We focused on the January-March period where the largest asymmetric pattern in trends was found. This analysis is based on the theory of linear interference of waves (Smith & Kushner, 2012), according to which a negative correlation exists between changes in the climatological stationary wavefield and the stratospheric jet strength.

First, we obtained the 2004–2021 climatology of the wave-1 component, after averaging the GPH over the [45°N, 70°N] latitude band. Then, we computed the linear trends of the wave-1 component over the same time period. Figure 9a shows the wave-1 climatology in colors and the respective linear trends (in m per decade) in contours. The position of the positive wave-1 GPH anomaly is approximately collocated with the region showing GPH negative trends and vice-versa for the negative anomaly. In particular, a 100/120° eastward shift between the

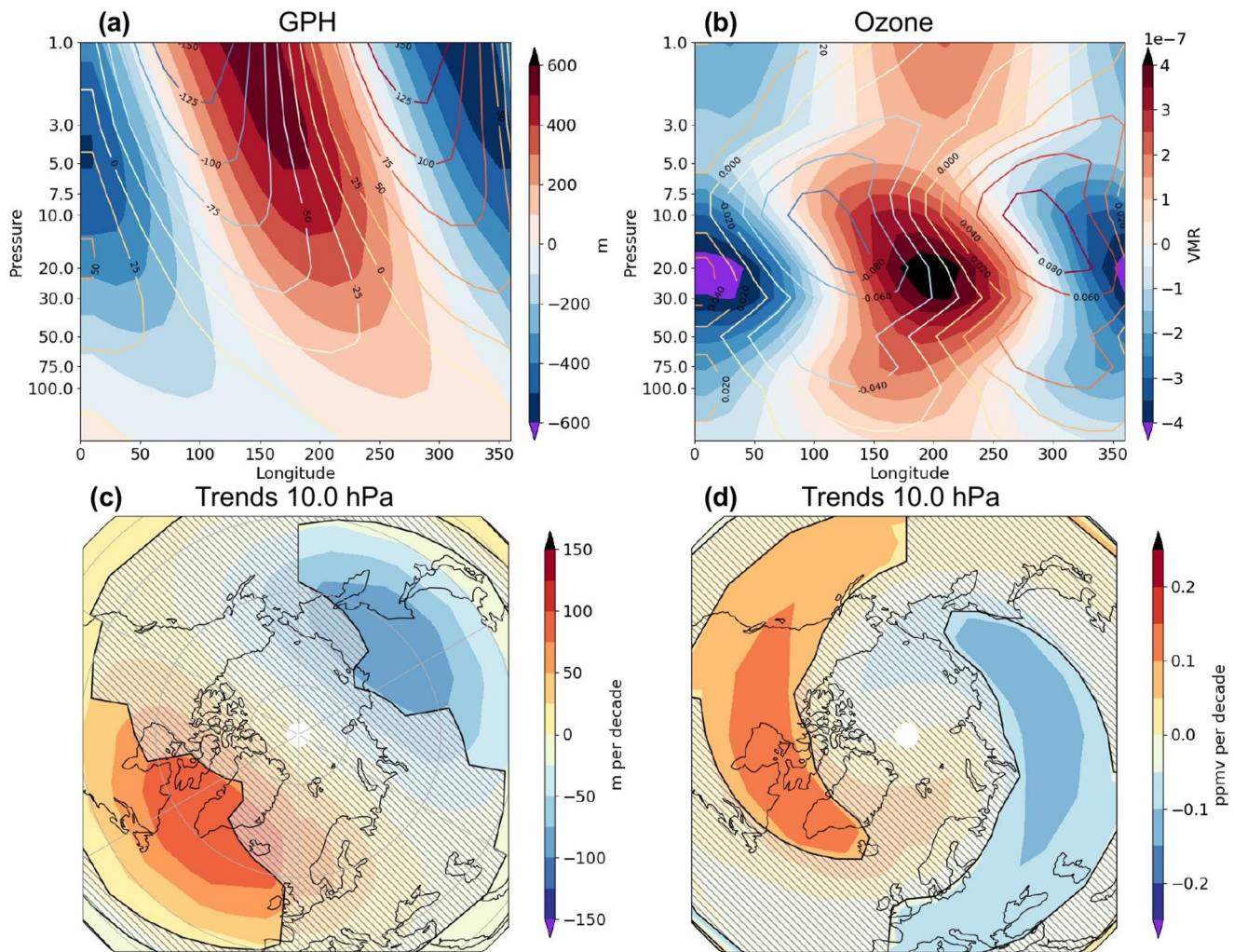


Figure 9. Top row, JFM climatology of the wave-1 component of GPH (left) and TOMCAT ozone (right) averaged over [45°N, 70°N]. The superimposed trends of the same quantities are shown as contours, with values in m per decade (left) and ppmv per decade (right). Bottom row, wave-1 trend values in each quantity at 10 hPa (striped regions indicate no statistical significance at 2σ).

climatology and the wave-1 trend maxima is visible, pointing out an eastward shift in the wave-1 forcing and a weakening of the wavenumber-1 planetary wave, according to the linear wave theory (Matsuno, 1970), over the last two decades.

We then performed a similar analysis for the ozone field, choosing the TOMCAT time series with a complete coverage of the polar regions. We find a similar baroclinic pattern in the climatology of the wave-1 component of TOMCAT ozone, particularly in the middle stratosphere as shown in Figure 9, panel (b). Above 5 hPa and below 50 hPa the correlation between the two panels breaks down. The trends of the ozone anomaly wave-1 component are superimposed in panel (b) in ppmv per decade. They are, similarly to GPH, out of phase with respect to their climatological values. Panels (c) and (d) show the GPH and ozone trends at 10.0 hPa, respectively, with the striped areas indicating values smaller than their 1σ uncertainty. The similarity is evident, although the shape of the two cores is more elongated for ozone trends.

As shown in Figure 10, a similar analysis was performed for the wave-2 components of ERA5 GPH and TOMCAT ozone anomalies. The climatologies of wave-2 GPH and ozone anomalies in the middle stratosphere again show a baroclinic structure, with values that are approximately in phase with their respective trends (about 30° east-shift between the two maxima or minima). This indicates that the wavenumber-2 wave forcing in the stratosphere has intensified in the last two decades. Panels (c) and (d) show the wave-2 GPH and ozone trends at

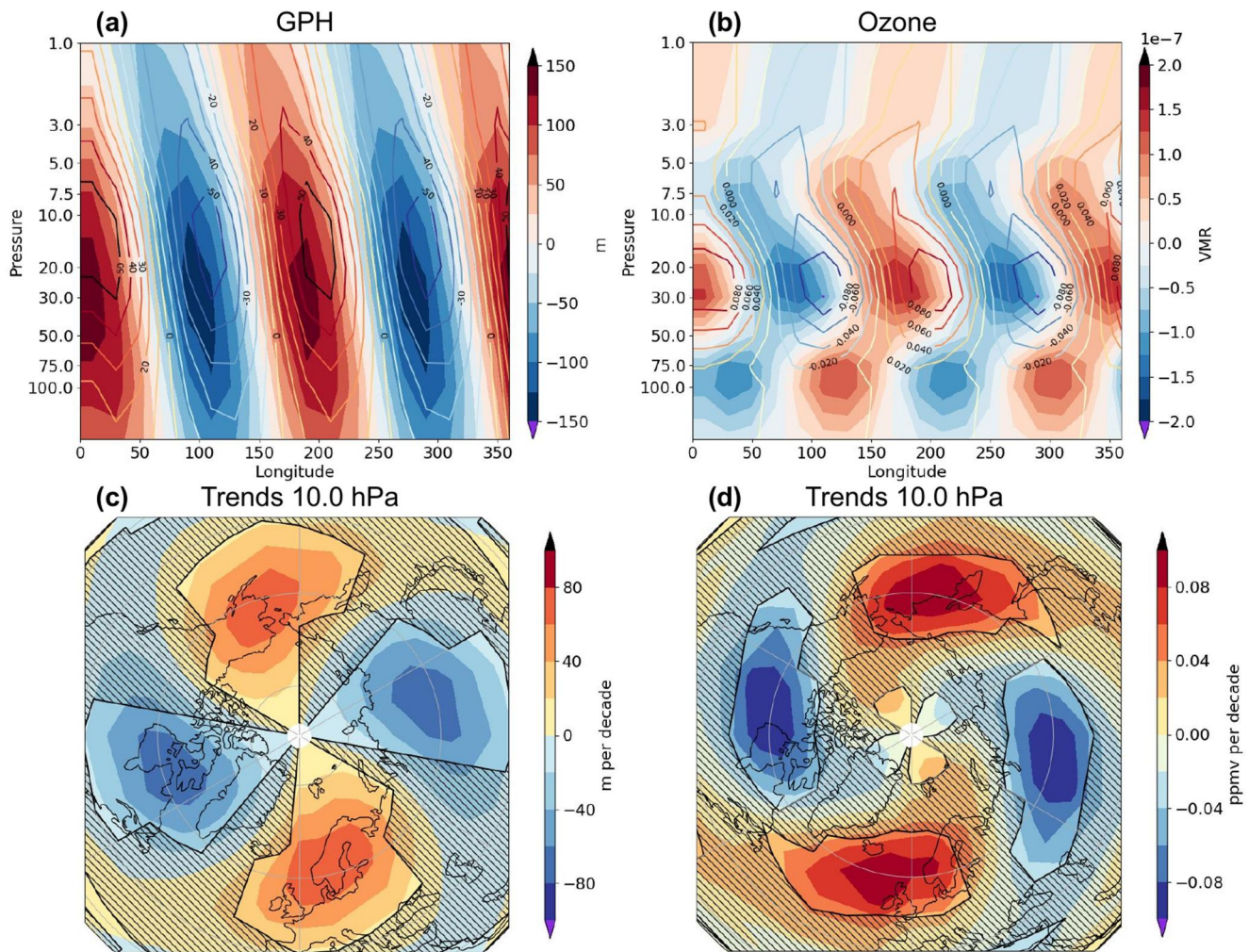


Figure 10. Same as Figure 9, but for the wave-2 components of GPH and ozone.

10.0 hPa, respectively. The similarity in this case is striking, however an angular shift with respect to each other is evident.

To quantify the correlation between climatology and trends, we calculated the pressure-weighted pattern correlation as in Fletcher and Kushner (2011) for the GPH pattern and found a correlation of -0.75 for wave-1, that is, out of phase, and 0.77 for wave-2, that is, close to in-phase. This analysis of the wave-1 and -2 components points to a strong correlation between changes in ozone and in GPH, which are themselves related to changes in wave activity. In our case, the pattern in GPH wave-1 and -2 components is consistent with a long-term shift and a strengthening of the polar vortex, as already pointed out by Hu et al. (2018). In fact, the weakening and shift of the wavenumber-1 planetary wave activity is leading to a strengthening of the polar vortex, partially offset by the strengthening of the wavenumber-2 wave activity. This seems to be the main driver of the asymmetry in the long-term ozone changes.

The identified GPH patterns are consistent with previous literature findings, for example, Hu et al. (2018), which the authors related to a weakening of the Aleutian low and to warmer sea-surface temperature over the central North Pacific. However other authors (e.g., Seviour, 2017; Zhang et al., 2016), pointed to a weakening of the polar vortex over the 1980–2010 period. In the next section we investigate changes in the polar vortex over the last four decades to reconcile these findings.

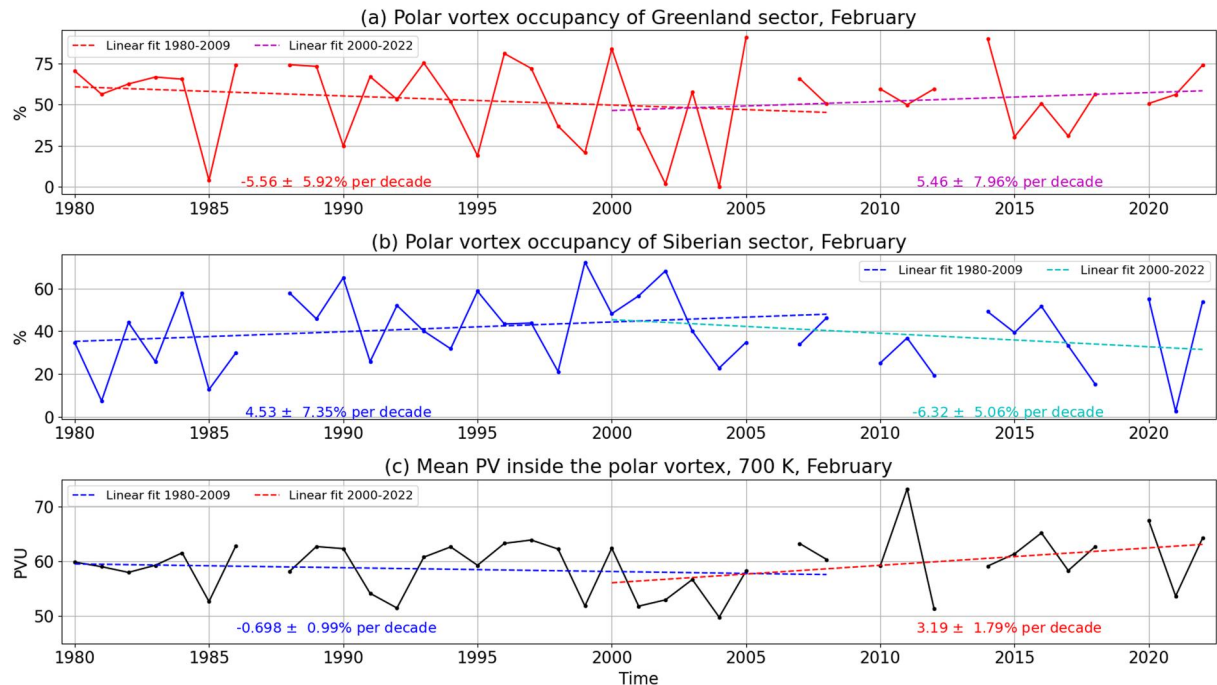


Figure 11. Panels (a) and (b) show the relative occupancy (%) of the Greenland sector and of the Siberian sector, respectively, by the polar vortex in February. Panel (c) shows the mean modified potential vorticity (PVU) within the polar vortex at the 700 K isentropic surface in February. The trends and their 1σ uncertainties are reported in the panels.

7. Potential Vorticity Trends and Polar Vortex Changes

We present now the changes in the polar vortex over the last four decades, following studies such as Zhang et al. (2016). We defined the polar vortex boundary using the methodology described in Nash et al. (1996); in particular, we used ERA5 modified potential vorticity at 700 K and wind on potential vorticity isolines. 700 K is considered to be representative of the middle stratosphere, around 30 km. The polar vortex boundary is based on the peak of the potential vorticity gradient in the equivalent latitude space (Butchart & Remsberg, 1986) collocated with a horizontal wind peak. After determining the polar vortex boundary for the Februaries since 1980, we investigated the change in its position and strength.

We defined two relevant sectors where the ozone asymmetric pattern is relevant: the first around Greenland and the second over Siberia, as shown in Figure S7 in Supporting Information S1. We define the polar vortex occupancy of a sector as the respective monthly mean areal fraction within the polar vortex boundary. We computed the relative occupancy of these two sectors in each February to assess decadal oscillations in the position of the polar vortex. As shown in Figure 11, a change in the linear trends of the sector occupancy during February occurred near the beginning of the century. Zhang et al. (2016) reported that over the period 1980–2009 the polar vortex underwent a shift to the Eurasian sector. However, from the beginning of the century our data indicate that an opposite shift seems to have occurred. This shift is not as robust as in the previous period, as several years (1987, 2006, 2009, 2013 and 2019) need to be screened out because of a weak polar vortex or major sudden stratospheric warming (SSW) event in February. As a result of the high interannual variability trends are mostly not significant even at 1σ level, as reported in the panels, and should be considered as decadal oscillations rather than a long-term change of the polar vortex.

The mean potential vorticity inside the polar vortex, shown in Figure 11, exhibits a negative linear trend in the first two decades. This is consistent with a weakening of the polar vortex as reported by Zhang et al. (2016) and Seviour (2017). During the final two decades, in contrast, the trend becomes positive, indicating a strengthening of the polar vortex as reported by Hu et al. (2018). The strengthening of the polar vortex is consistent with a positive shift in the Arctic oscillation (Weber et al., 2022).

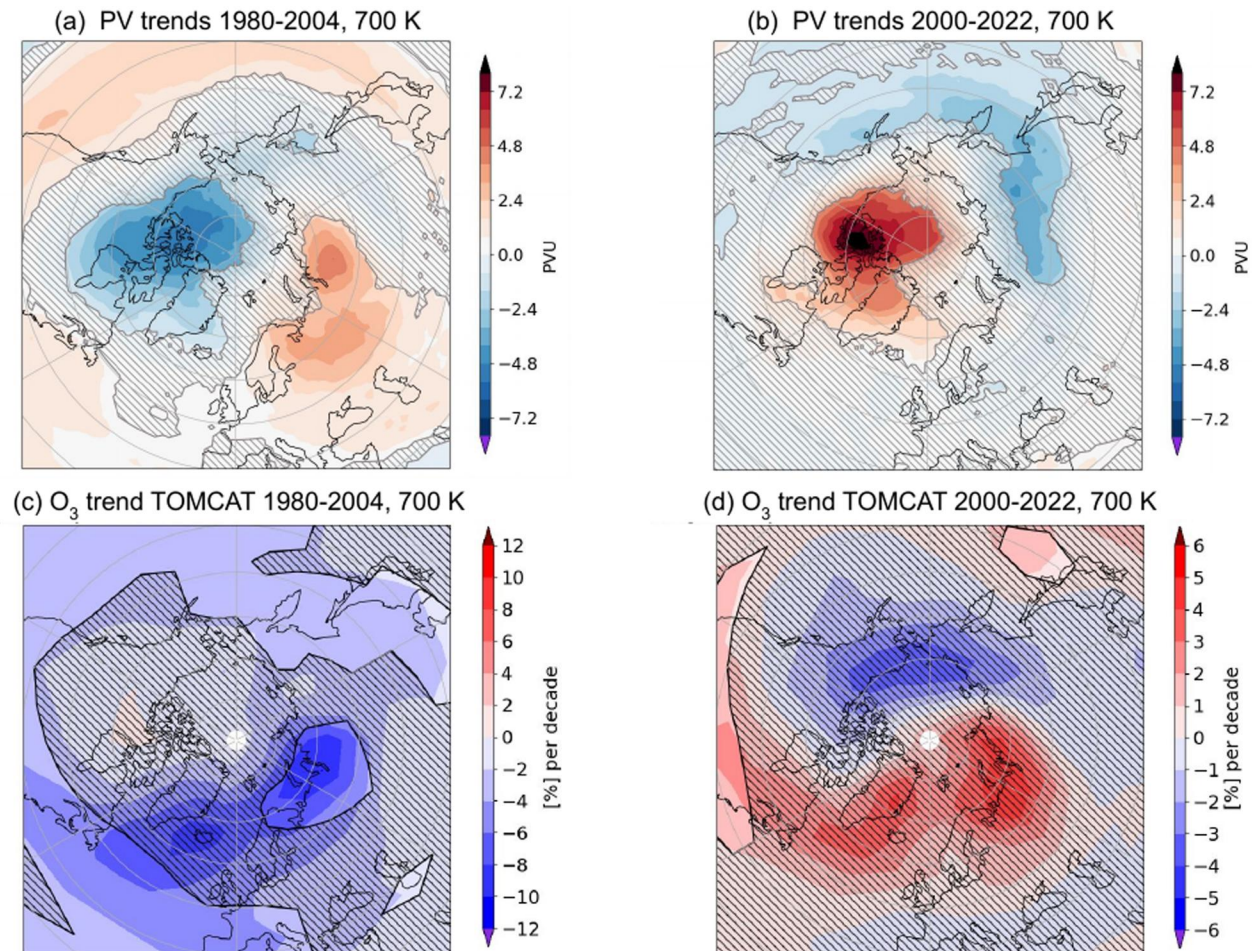


Figure 12. Trends of the ERA5 modified potential vorticity (panels a and b) and of the TOMCAT ozone (panels c and d) at the 700 K isentropic surface are shown for the periods 1980–2005 and 2000–2022.

Finally, we investigate the trends of the modified potential vorticity in the middle stratosphere (700 K) over the two periods 1980–2004 and 2000–2022. In the top panels of Figure 12, we clearly see a reversal of the pattern over the polar regions, with panel (a) showing a shift of the polar vortex to Eurasia similar to the findings of Zhang et al. (2016). Panel (b) indicates a shift of its mean position again toward North America over the last 20 years. Looking at the ozone trends on the 700 K isentropic surface from the TOMCAT time series in the respective periods, shown in the bottom row of Figure 12, we also note a reversal of the pattern. The negative values were largest over the Atlantic/Scandinavian sector during the first period and positive values were largest in the same region during the second period.

8. Conclusions

In this study we have presented a comparison between satellite limb observations and simulations from the TOMCAT CTM to investigate the zonal asymmetry in ozone trends identified at northern high latitudes. The OMPS-LP product has been recently updated at the University of Bremen by using the improved L1G data provided by the NASA team, leading to improved long-term stability of the ozone time series with respect to the previous version. A preliminary comparison between SCIA + OMPS and TOMCAT time series and zonal trends demonstrated the overall good agreement between the two when considering deseasonalized anomalies. We then presented the longitudinal asymmetry in trends observed at northern high latitudes over the period 2004–2021, which is well captured not only by the CTM but also by the ERA5 time series, hinting at the dynamical origin of this feature.

By using dedicated TOMCAT runs we further showed that the identified patterns are dynamically driven, as neither gas-phase nor heterogeneous chemistry was found to have a direct role in the discussed asymmetry. Ozone trends divided by season indicate that this asymmetry has the largest amplitude in late winter/early spring. In this season we found positive values of up to 6%–7% per decade over Greenland and negative values of 3%–4% per decade over Eurasia. This seasonal trend pattern observed in SCIA + OMPS is reproduced very well by TOMCAT.

We decomposed ERA5 geopotential height (GPH) and TOMCAT ozone fields in wave-1 and -2 components for winter months JFM, finding a strong similarity in the changes of the two quantities in the middle stratosphere. Assuming linear wave superposition, the findings are consistent with a long-term shift and a strengthening of the polar vortex, that is, a weakening of the wavenumber-1 planetary wave. In this way we could link the zonal asymmetric pattern in ozone trends to changes in the wave activity in the stratosphere.

The analysis of the polar vortex position and trends in potential vorticity in the middle stratosphere (Sect. 7) qualitatively confirms the suggested relationship between the shift in the mean polar vortex position and the ozone trend asymmetry. The overall pattern underwent decadal changes over the last 40 years, with the most recent two decades seeing a probable strengthening of the vortex and a shift toward North America. This final section of the manuscript is related to the study of the long-term variations of the polar vortex due to climate change and requires further investigations to understand its causes.

In summary, this study has highlighted the role of decadal variations in atmospheric dynamics in explaining ozone trends at northern high latitudes. The observed asymmetry of ozone trends during the past decades is a consequence of decadal climate variability originating in the troposphere. This asymmetric pattern should be taken into account when calculating ozone trends in the polar region in particular when using ground-based observations, such as ozonesondes and Fourier transform infrared spectrometers.

Appendix A: Methods to Merge SCIAMACHY and OMPS-LP Data Sets

Two approaches have been employed for the study of seasonal trends. In the first case we compute the seasonal averages of the merged monthly SCIA + OMPS data set. In the second case the merging is applied to seasonal averages of both data set anomalies. A filtering is necessary to remove latitude bins for which some months in the defined season are unavailable or when the latitude coverage of the two instruments differs (at high latitudes). It was found that the second method provides better agreement with CTM simulations compared to the first approach.

This agreement is illustrated using, as an example, the March–April (MA) trends at 32 km displayed in Figure A1. The “SCIA + OMPS post” indicates the computation of seasonal averages using the merged monthly data set (first method), whereas the “SCIA + OMPS pre” in the middle panel indicates the merging performed on seasonal averages (second method). The comparison with TOMCAT significantly improves in the second case.

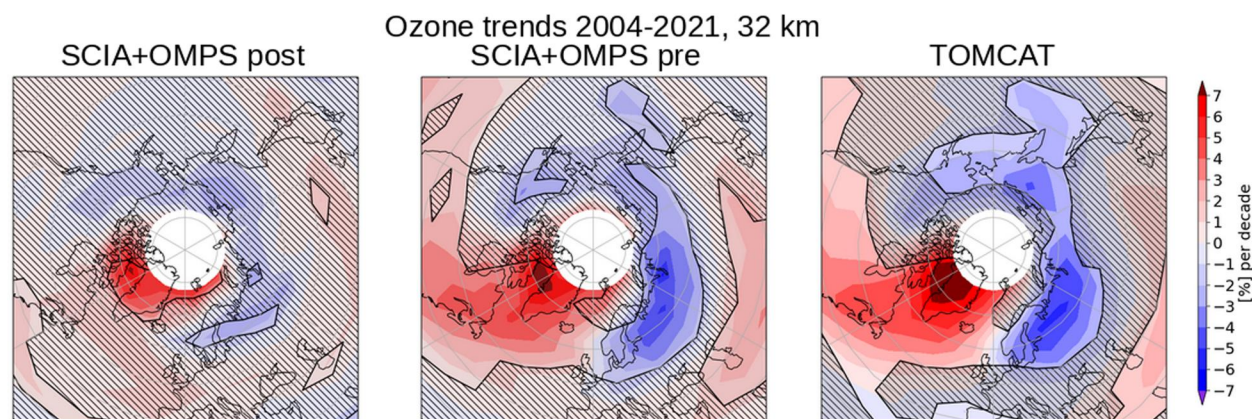


Figure A1. Comparison of seasonal ozone trends in months MA at 32 km from SCIA + OMPS (left and center panels) and TOMCAT (right panel). In the left panel monthly time series of the two satellite data sets were merged. In the central panel averaged seasonal values were merged.

Data Availability Statement

The Merged SCIA + OMPS data set produced at the University of Bremen and used for this study is available for download (Arosio & Rozanov, 2023). TOMCAT simulations (Arosio & Chipperfield, 2023) as well as the extracted PV and GPH values used for this study (Arosio, 2023) are also available.

Acknowledgments

This study was supported by the University and state of Bremen, the ESA Living Planet Fellowship SOLVE and the PRIME programme of the German Academic Exchange Service (DAAD). The DAAD support in particular allowed CA to be a visiting research fellow at the University of Leeds and at NASA, and to develop this project. The study is also within the framework of the ESA Ozone Recovery from Merged Observational Data and Model Analysis (OREGANO) project, which involves, among others, the University of Bremen and of Leeds. We would like to acknowledge the NASA OMI-SIPS team, in particular Natalya Kramarova, for the helpful collaboration during the testing and release phase of the OMPS-LP L1G v2.6 data, as well as the GMAO team for providing the M2-GMI product. The development of the aerosol data set required to retrieve the ozone data used in this study was funded by the German Research Foundation (DFG) via the Research Unit VollImpact (Grant FOR2820). The authors gratefully acknowledge the computing time granted by the Resource Allocation Board and provided on the supercomputer Lise and Emmy at NHR ZIB and NHR Goettingen as part of the NHR infrastructure. The calculations for this research were conducted with computing resources under the projects hbk00062 and hbk00098. The GALAHAD Fortran Library was used for calculations. The modeling work at Leeds was supported by the NERC grant NE/V011863/1. Open Access funding enabled and organized by Projekt DEAL.

References

- Arosio, C. (2023). Extracted PV and GPH data from ECMWF-ERA5 [Dataset]. *Zenodo*. <https://doi.org/10.5281/zenodo.10054575>. Accessed: 24 02 2024
- Arosio, C., & Chipperfield, M. (2023). TOMCAT simulations [Dataset]. *Zenodo*. <https://doi.org/10.5281/zenodo.10054832>. Accessed: 24 02 2024
- Arosio, C., & Rozanov, A. (2023). Merged SCIA+OMPS time series [Dataset]. *Zenodo*. <https://doi.org/10.5281/zenodo.10033299>. Accessed: 24 02 2024
- Arosio, C., Rozanov, A., Malinina, E., Weber, M., & Burrows, J. P. (2019). Merging of ozone profiles from SCIAMACHY, OMPS and SAGE II observations to study stratospheric ozone changes. *Atmospheric Measurement Techniques*, 12(4), 2423–2444. <https://doi.org/10.5194/amt-12-2423-2019>
- Ball, W. T., Alsing, J., Mortlock, D. J., Staehelin, J., Haigh, J. D., Peter, T., et al. (2018). Evidence for a continuous decline in lower stratospheric ozone offsetting ozone layer recovery. *Atmospheric Chemistry and Physics*, 18(2), 1379–1394. <https://doi.org/10.5194/acp-18-1379-2018>
- Bari, D., Gabriel, A., Körnich, H., & Peters, D. (2013). The effect of zonal asymmetries in the Brewer-Dobson circulation on ozone and water vapor distributions in the northern middle atmosphere. *Journal of Geophysical Research: Atmospheres*, 118(9), 3447–3466. <https://doi.org/10.1029/2012jd017709>
- Bernet, L., Boyd, I., Nedoluha, G., Querel, R., Swart, D., & Hocke, K. (2020). Validation and trend analysis of stratospheric ozone data from ground-based observations at Lauder, New Zealand. *Remote Sensing*, 13(1), 109. <https://doi.org/10.3390/rs13010109>
- Butchart, N. (2014). The Brewer-Dobson circulation. *Reviews of Geophysics*, 52(2), 157–184. <https://doi.org/10.1002/2013rg000448>
- Butchart, N., & Remsberg, E. E. (1986). The area of the stratospheric polar vortex as a diagnostic for tracer transport on an isentropic surface. *Journal of the Atmospheric Sciences*, 43(13), 1319–1339. [https://doi.org/10.1175/1520-0469\(1986\)043<1319:taotsp>2.0.co;2](https://doi.org/10.1175/1520-0469(1986)043<1319:taotsp>2.0.co;2)
- Chipperfield, M. (2006). New version of the TOMCAT/SLIMCAT off-line chemical transport model: Intercomparison of stratospheric tracer experiments. *Quarterly Journal of the Royal Meteorological Society: A journal of the atmospheric sciences, applied meteorology and physical oceanography*, 132(617), 1179–1203. <https://doi.org/10.1256/qj.05.51>
- Chipperfield, M., Dhomse, S., Hossaini, R., Feng, W., Santee, M. L., Weber, M., et al. (2018). On the cause of recent variations in lower stratospheric ozone. *Geophysical Research Letters*, 45(11), 5718–5726. <https://doi.org/10.1029/2018gl078071>
- Coldewey-Egbers, M., Loyola R, D. G., Lerot, C., & van Roozendaal, M. (2022). Global, regional and seasonal analysis of total ozone trends derived from the 1995-2020 GTO-ECV climate data record. *Atmospheric Chemistry and Physics*, 22(10), 6861–6878. <https://doi.org/10.5194/acp-22-6861-2022>
- Dhomse, S. S., Arosio, C., Feng, W., Rozanov, A., Weber, M., & Chipperfield, M. P. (2021). ML-TOMCAT: Machine-learning-based satellite-corrected global stratospheric ozone profile data set from a chemical transport model. *Earth System Science Data*, 13(12), 5711–5729. <https://doi.org/10.5194/essd-13-5711-2021>
- Fletcher, C. G., & Kushner, P. J. (2011). The role of linear interference in the annular mode response to tropical SST forcing. *Journal of Climate*, 24(3), 778–794. <https://doi.org/10.1175/2010jcli3735.1>
- Galytska, E., Rozanov, A., Chipperfield, M. P., Dhomse, S. S., Weber, M., Arosio, C., et al. (2019). Dynamically controlled ozone decline in the tropical mid-stratosphere observed by SCIAMACHY. *Atmospheric Chemistry and Physics*, 19(2), 767–783. <https://doi.org/10.5194/acp-19-767-2019>
- Garcia, R. R., & Randel, W. J. (2008). Acceleration of the Brewer–Dobson circulation due to increases in greenhouse gases. *Journal of the Atmospheric Sciences*, 65(8), 2731–2739. <https://doi.org/10.1175/2008jas2712.1>
- Godin-Beekmann, S., Azouz, N., Sofieva, V. F., Hubert, D., Petropavlovskikh, I., Effertz, P., et al. (2022). Updated trends of the stratospheric ozone vertical distribution in the 60° S–60° N latitude range based on the LOTUS regression model. *Atmospheric Chemistry and Physics*, 22(17), 11657–11673. <https://doi.org/10.5194/acp-22-11657-2022>
- Groves, K., Mattingly, S., & Tuck, A. (1978). Increased atmospheric carbon dioxide and stratospheric ozone. *Nature*, 273(5665), 711–715. <https://doi.org/10.1038/273711a0>
- Hood, L., & Zaff, D. A. (1995). Lower stratospheric stationary waves and the longitude dependence of ozone trends in winter. *Journal of Geophysical Research*, 100(D12), 25791–25800. <https://doi.org/10.1029/95jd01943>
- Hu, D., Guan, Z., Tian, W., & Ren, R. (2018). Recent strengthening of the stratospheric Arctic vortex response to warming in the central North Pacific. *Nature Communications*, 9(1), 1697. <https://doi.org/10.1038/s41467-018-04138-3>
- Hubert, D., Lambert, J.-C., Verhoelst, T., Granville, J., Keppens, A., Baray, J.-L., et al. (2016). Ground-based assessment of the bias and long-term stability of 14 limb and occultation ozone profile data records. *Atmospheric Measurement Techniques*, 9(6), 2497–2534. <https://doi.org/10.5194/amt-9-2497-2016>
- Karpechko, A. Y., Afargan-Gerstman, H., Butler, A. H., Domeisen, D. I., Kretschmer, M., Lawrence, Z., et al. (2022). Northern hemisphere stratosphere-troposphere circulation change in CMIP6 models: 1. Inter-model spread and scenario sensitivity. *Journal of Geophysical Research: Atmospheres*, 127(18), e2022JD036992. <https://doi.org/10.1029/2022jd036992>
- Kozubek, M., Krizan, P., & Lastovicka, J. (2015). Northern hemisphere stratospheric winds in higher midlatitudes: Longitudinal distribution and long-term trends. *Atmospheric Chemistry and Physics*, 15(4), 2203–2213. <https://doi.org/10.5194/acp-15-2203-2015>
- Kozubek, M., Krizan, P., & Lastovicka, J. (2017). Comparison of the long-term trends in stratospheric dynamics of four reanalyses. *Annales Geophysicae*, 35(2), 279–294. <https://doi.org/10.5194/angeo-35-279-2017>
- Kramarova, N. A., Bhartia, P. K., Jaross, G., Moy, L., Xu, P., Chen, Z., et al. (2018). Validation of ozone profile retrievals derived from the OMPS LP version 2.5 algorithm against correlative satellite measurements. *Atmospheric Measurement Techniques*, 11(5), 2837–2861. <https://doi.org/10.5194/amt-11-2837-2018>
- Li, Y., Dhomse, S. S., Chipperfield, M. P., Feng, W., Bian, J., Xia, Y., & Guo, D. (2023). Stratospheric ozone trends and attribution over 1984–2020 using ordinary and regularised multivariate regression models. *EGU sphere*, 2023, 1–24.

- Li, Y., Dhomse, S. S., Chipperfield, M. P., Feng, W., Chrysanthou, A., Xia, Y., & Guo, D. (2022). Effects of reanalysis forcing fields on ozone trends and age of air from a chemical transport model. *Atmospheric Chemistry and Physics*, 22(16), 10635–10656. <https://doi.org/10.5194/acp-22-10635-2022>
- Lu, J., Lou, S., Huang, X., Xue, L., Ding, K., Liu, T., et al. (2023). Stratospheric aerosol and ozone responses to the Hunga Tonga-Hunga Ha'apai volcanic eruption. *Geophysical Research Letters*, 50(4), e2022GL102315. <https://doi.org/10.1029/2022gl102315>
- Matsuno, T. (1970). Vertical propagation of stationary planetary waves in the winter Northern Hemisphere. *Journal of the Atmospheric Sciences*, 27(6), 871–883. [https://doi.org/10.1175/1520-0469\(1970\)027<0871:vpospw>2.0.co;2](https://doi.org/10.1175/1520-0469(1970)027<0871:vpospw>2.0.co;2)
- McIntyre, M., & Palmer, T. (1984). The 'surf zone' in the stratosphere. *Journal of Atmospheric and Terrestrial Physics*, 46(9), 825–849. [https://doi.org/10.1016/0021-9169\(84\)90063-1](https://doi.org/10.1016/0021-9169(84)90063-1)
- Nash, E. R., Newman, P. A., Rosenfield, J. E., & Schoeberl, M. R. (1996). An objective determination of the polar vortex using Ertel's potential vorticity. *Journal of Geophysical Research*, 101(D5), 9471–9478. <https://doi.org/10.1029/96jd00066>
- Peters, D., & Entzian, G. (1999). Longitude-dependent decadal changes of total ozone in boreal winter months during 1979–92. *Journal of Climate*, 12(4), 1038–1048. [https://doi.org/10.1175/1520-0442\(1999\)012<1038:lddcot>2.0.co;2](https://doi.org/10.1175/1520-0442(1999)012<1038:lddcot>2.0.co;2)
- Petrovavlovskikh, I., Godin-Beekmann, S., Hubert, D., Damadeo, R., Hassler, B., & Sofieva, V. (2019). SPARC/IO3C/GAW report on long-term ozone trends and uncertainties in the stratosphere (vols. SPARC report No. 9, WCRP-17/2018, GAW report No. 241). <https://doi.org/10.17874/f899e57a20b>
- Seinfeld, J. H., & Pandis, S. N. (2016). *Atmospheric chemistry and physics: From air pollution to climate change*. John Wiley and Sons.
- Seviour, W. J. (2017). Weakening and shift of the Arctic stratospheric polar vortex: Internal variability or forced response? *Geophysical Research Letters*, 44(7), 3365–3373. <https://doi.org/10.1002/2017gl073071>
- Simmons, A., Poli, P., Dee, D., Berrisford, P., Hersbach, H., Kobayashi, S., & Peubey, C. (2014). Estimating low-frequency variability and trends in atmospheric temperature using ERA-Interim. *Quarterly Journal of the Royal Meteorological Society*, 140(679), 329–353. <https://doi.org/10.1002/qj.2317>
- Smith, K. L., & Kushner, P. J. (2012). Linear interference and the initiation of extratropical stratosphere-troposphere interactions. *Journal of Geophysical Research*, 117(D13). <https://doi.org/10.1029/2012jd017587>
- Sofieva, V. F., Kyrölä, E., Laine, M., Tamminen, J., Degenstein, D., Bourassa, A., et al. (2017). Merged SAGE II, Ozone_cci and OMPS ozone profile dataset and evaluation of ozone trends in the stratosphere. *Atmospheric Chemistry and Physics*, 17(20), 12533–12552. <https://doi.org/10.5194/acp-17-12533-2017>
- Sofieva, V. F., Szelag, M., Tamminen, J., Kyrölä, E., Degenstein, D., Roth, C., et al. (2021). Measurement report: Regional trends of stratospheric ozone evaluated using the Merged GRIdded dataset of ozone profiles (MEGRIDOP). *Atmospheric Chemistry and Physics*, 21(9), 6707–6720. <https://doi.org/10.5194/acp-21-6707-2021>
- Waugh, D., Oman, L., Kawa, S., Stolarski, R., Pawson, S., Douglass, A., et al. (2009). Impacts of climate change on stratospheric ozone recovery. *Geophysical Research Letters*, 36(3). <https://doi.org/10.1029/2008gl036223>
- Weber, M., Arosio, C., Coldewey-Egbers, M., Fioletov, V. E., Frith, S. M., Wild, J. D., et al. (2022). Global total ozone recovery trends attributed to ozone-depleting substance (ODS) changes derived from five merged ozone datasets. *Atmospheric Chemistry and Physics*, 22(10), 6843–6859. <https://doi.org/10.5194/acp-22-6843-2022>
- WMO. (2018). *Scientific assessment of ozone depletion 2018, global ozone research and monitoring project report 58*. World Meteorological Organization. Retrieved from <https://csl.noaa.gov/assessments/ozone/2018/downloads/2018OzoneAssessment.pdf>
- WMO. (2022). *Scientific assessment of ozone depletion 2022, global ozone research and monitoring project report 59*. World Meteorological Organization. Retrieved from <https://csl.noaa.gov/assessments/ozone/2022/downloads/2022OzoneAssessment.pdf>
- Zhang, J., Tian, W., Chipperfield, M. P., Xie, F., & Huang, J. (2016). Persistent shift of the Arctic polar vortex towards the Eurasian continent in recent decades. *Nature Climate Change*, 6(12), 1094–1099. <https://doi.org/10.1038/nclimate3136>